

## Article

# Study on Fluctuating Wind Characteristics and Non-Stationarity at U-Shaped Canyon Bridge Site

Zhe Sun, Zhuoyi Zou, Jiaying Wang \*, Xue Zhao  and Feng Wang 

School of Highway, Chang'an University, Xi'an 710064, China; zhesun@chd.edu.cn (Z.S.); zouzy@chd.edu.cn (Z.Z.); 2021021021@chd.edu.cn (X.Z.); wf@chd.edu.cn (F.W.)

\* Correspondence: wjying@chd.edu.cn

**Abstract:** To investigate the non-stationary characteristics of the wind field at the U-shaped canyon bridge site and its impact on fluctuating wind characteristics, a wind observation tower was installed near a cable-stayed bridge. The Augmented Dickey–Fuller (ADF) test was employed to assess the stationarity of wind speed series, while the discrete wavelet transform (DWT) was applied to reconstruct the time-varying mean wind and analyze its effect on fluctuating wind characteristics. Results indicate that wind speeds in this region exhibit bimodal distribution characteristics, with the Weibull–Gamma mixed distribution model providing the best fit. The proportion of non-stationary samples increases with height. Autocorrelation function (ACF), partial autocorrelation function (PACF) tests, and power spectral density (PSD) analysis determined the optimal wavelet decomposition level for wind speed in this region. Analysis of non-stationary samples using db10 wavelet reconstruction reveals that the stationary wind speed model overestimates turbulence intensity but underestimates the turbulence integral scale. The downwind spectrum deviates from the Kaimal spectrum in both low- and high-frequency bands, whereas the vertical spectrum aligns well with the Panofsky spectrum. The findings demonstrate that the wavelet reconstruction method more accurately captures fluctuating wind characteristics under the complex terrain conditions of this canyon area.

**Keywords:** field measurement; fluctuating wind; non-stationary wind; wavelet reconstruction



Academic Editor: Andreas Fischer

Received: 16 January 2025

Revised: 26 January 2025

Accepted: 29 January 2025

Published: 31 January 2025

**Citation:** Sun, Z.; Zou, Z.; Wang, J.; Zhao, X.; Wang, F. Study on Fluctuating Wind Characteristics and Non-Stationarity at U-Shaped Canyon Bridge Site. *Appl. Sci.* **2025**, *15*, 1482. <https://doi.org/10.3390/app15031482>

**Copyright:** © 2025 by the authors. Licensee MDPI, Basel, Switzerland. This article is an open access article distributed under the terms and conditions of the Creative Commons Attribution (CC BY) license (<https://creativecommons.org/licenses/by/4.0/>).

## 1. Introduction

Advancements in bridge construction technology and equipment have led to the construction of an increasing number of long-span cable bridges in canyon areas. However, due to their flexible structures, long-span bridges are highly susceptible to wind effects. Accurately estimating wind characteristics is essential for studying the wind response of structures [1–3]. Long-span bridges, predominantly located in mountainous and canyon areas, are frequently impacted by strong canyon winds [4,5]. Complex terrain and climatic conditions cause wind parameters to exhibit significant non-stationary characteristics, posing challenges to the safety and performance of wind-sensitive infrastructure such as long-span bridges, tall structures, and wind power generation facilities.

Research on mountain canyon wind fields primarily relies on field measurements [6], wind tunnel tests [7], and numerical simulations [8]. Field measurements are the most direct and reliable method. Although field measurements require significant investment and time, and have certain limitations, they provide reliable and accurate data, often used to validate other methods, making them widely favored for analyzing wind field characteristics. Song et al. [9] evaluated the wind field characteristics in the Y-shaped canyon by combining wind

tunnel test results with field measurement data. It is found that the wind characteristics under complex terrain show significant sensitivity to the wind direction, and the local terrain has considerable influence on the wind field. He et al. [10] introduced fractal dimensions to quantify wind parameter fluctuations, analyzed gust factors under various terrain conditions, and conducted a comparative study. Zhang et al. [11] used an ultrasonic anemometer to investigate the influence of wind direction on the characteristic parameters of deep canyon winds. They found significant directional variations in parameters such as the turbulence integral scale. Additionally, wind speed, turbulence intensity, and turbulence integral scale followed a lognormal distribution across all directions, while the angle of attack adhered to a normal distribution. Ren et al. [12] installed five anemometers along the bridge span for long-term field measurements, revealing that the valley wind field is heavily influenced by terrain and exhibits strong non-stationarity. Jing et al. [13] analyzed and compared wind characteristics in mountainous areas using data from two wind towers, one on a mountainside and the other at a canyon bottom. They found that mean wind speed, turbulence intensity, and wind power spectra could not be accurately predicted by existing norms or standards and proposed an exponential coherence model to effectively describe vertical coherence.

Numerous studies have demonstrated that mountain winds exhibit non-stationary characteristics [14,15], prompting extensive discussions on wind field non-stationarity under varying terrain conditions and its impact on structural wind resistance design. Guo et al. [16] compared the non-stationarity of mountain canyon winds with normal climate winds under identical sample lengths and observation intervals. They found that when the sample length exceeded 10 min, the probability distribution of the non-stationarity index showed significant differences between the two. Niu et al. [17] observed that near-surface wind fields below 10 m in hilly areas exhibited non-stationary characteristics. They also noted that stationary models tend to overestimate both turbulence intensity and turbulence integral scale. Xin et al. [18] employed the statistical Augmented Dickey–Fuller (ADF) method to quantitatively assess the non-stationarity of measured wind speed samples and discovered that abrupt winds could occur in mountainous terrain. While existing studies have explored the characteristics and effects of wind fields in complex terrains from various perspectives, the applicability of current methods to non-stationary wind speed models remains limited. Ren et al. [12] analyzed wind sample non-stationarity using running tests and wavelet analysis. Their findings revealed that wind field characteristics in non-stationary wind speed models deviated from the recommended values in existing standards. Zhou et al. [19] investigated the non-stationary characteristics of plateau winds through experiments. They found that turbulence intensity and gust factors in plateau winds were significantly higher than those in plain areas. Lou et al. [20] highlighted the importance of selecting appropriate models for wind field analysis in complex terrains by comparing stationary models with various non-stationary models.

Currently, few studies focus on non-stationary winds in canyon areas, and the specific effects of such winds on fluctuating wind characteristics in mountainous regions remain unclear. Conducting in-depth analyses and discussions based on measured data is urgently needed to provide references for the wind resistance design of mountain structures. Using wind speed measurement data from a mountain bridge site, this study systematically analyzes the pulsating wind effects in canyon areas.

This study aims to examine the non-stationary characteristics of wind fields in complex terrains and their effects on turbulence intensity, wind power spectra, and related parameters, thereby enriching measured data and analysis results for canyon wind fields. Section 2 outlines the equipment and layout used for wind field measurements. Section 3 analyzes the non-stationary characteristics of wind speed and the statistical properties of pulsating

winds. It also compares pulsating wind characteristics across different wind speed models using turbulence intensity and gust factor results. Section 4 extracts the time-varying mean wind using discrete wavelet transform, analyzes fluctuating wind characteristics, proposes optimal decomposition layers, and verifies the effectiveness of wavelet decomposition.

## 2. Wind Field Measurement

The U-shaped canyon station is located at the site of a cable-stayed bridge in Lijiang City, Yunnan Province, China. The bridge site is situated in a mountainous forest with undulating topography. The layout of the wind observation tower at the bridge site is illustrated in Figure 1. Ultrasonic anemometers are well-suited for long-term wind measurements in bridges and mountainous areas, offering distinct advantages over other types of sensors [21]. Windsonic M two-dimensional ultrasonic wind sensors, manufactured by Gill Instruments Limited (Lymington, UK), were installed at heights of 10 m, 20 m, 30 m, and 40 m above the ground. These devices have a wind speed measurement range of 0–60 m/s and a measurement uncertainty of  $\pm 2\%$ . A WindMaster HS 3D anemometer, also manufactured by Gill Instruments Limited (UK), was installed 50 m away. This instrument has a wind speed range of 0–45 m/s, a resolution of 0.01 m/s, measurement uncertainty less than 1.5%, and the upper frequency limit of the anemometer can reach 32 Hz. The wind speed data output frequency for all instruments was set to 4 Hz. The coordinate system is defined as such that the U direction aligns with the transverse bridge axis (across the bridge), the V direction corresponds to the longitudinal bridge axis (along the bridge), and the W direction represents the vertical axis.

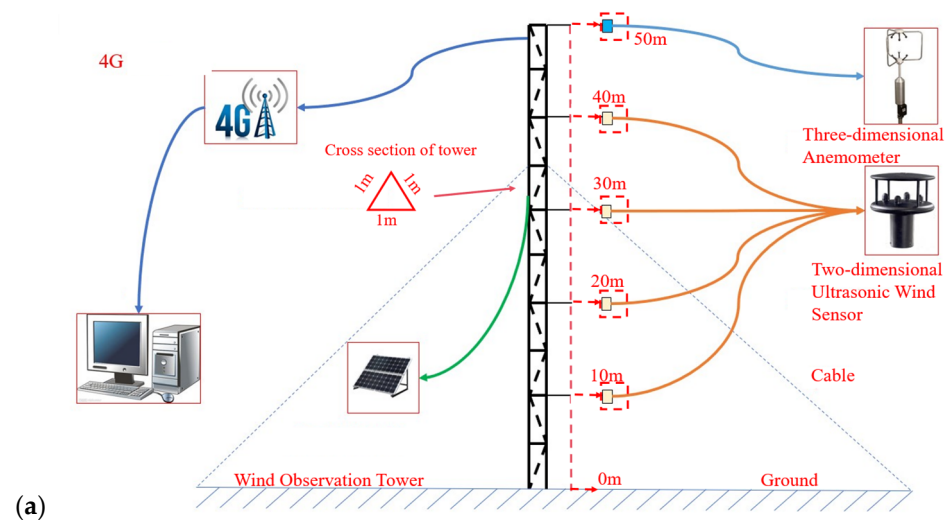
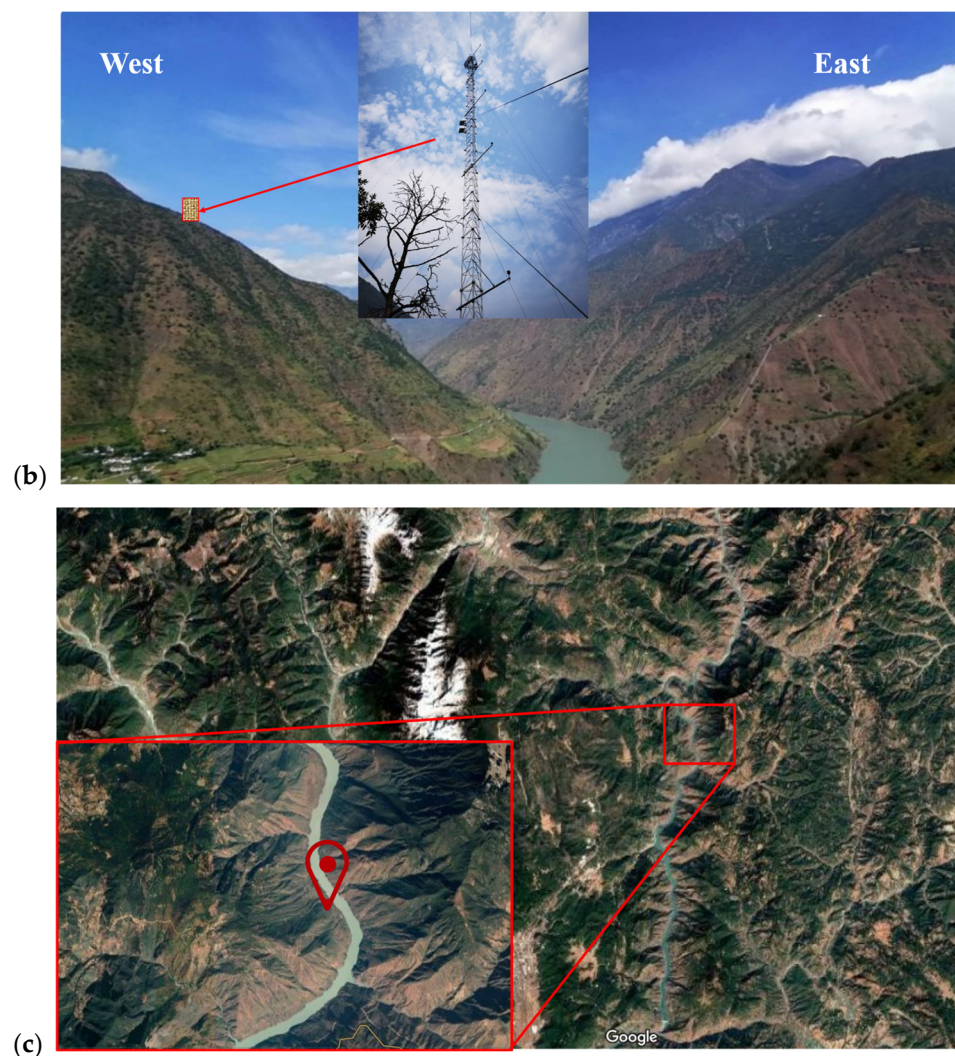


Figure 1. Cont.



**Figure 1.** Layout of wind tower at U-shaped canyon bridge site.

### 3. Analysis of Fluctuating Wind Characteristics

#### 3.1. Non-Stationarity Theory and Analysis Method

In wind engineering, wind speed is typically divided into mean wind and fluctuating wind under the assumption of stationarity, mathematically expressed as follows:

$$U(t) = \bar{U}(t) + u(t) \quad (1)$$

$U(t)$  represents the measured wind speed,  $\bar{U}(t)$  represents the mean wind speed within the time period, and  $u(t)$  is the fluctuating wind speed.

A wind speed series  $\{X_t\}$  is considered stationary if its statistical properties remain constant over time. The stationary model assumes that wind speed follows a stationary random process. This assumption is often valid in flat terrain. However, the stationary model is applicable only when wind speed characteristics do not exhibit statistically significant variations over time. In complex mountainous terrains, wind field changes often exhibit pronounced non-stationary characteristics.

The non-stationary model decomposes wind speed into a time-varying mean wind and a fluctuating component, defined as the difference between the measured wind speed and the time-varying mean wind:

$$U(t) = \bar{U}^*(t) + u^*(t) \quad (2)$$

$U(t)$  represents the measured wind speed,  $U^*(t)$  represents the time-varying mean wind, and  $u^*(t)$  is the fluctuating wind.

Selecting an appropriate wind speed model is crucial for analyzing wind characteristics. Stationarity tests play a key role in selecting appropriate wind speed models. Common methods for assessing time series stationarity include the following:

**Unit Root Tests:** The Augmented Dickey–Fuller (ADF) test extends the original Dickey–Fuller test and is suitable for higher-order autoregressive processes.

**KPSS Test:** The Kwiatkowski–Phillips–Schmidt–Shin test assumes stationarity as the null hypothesis, contrasting with unit root tests.

**Runs Test:** This detects random patterns in a time series to indirectly infer stationarity.

**Coefficient of Variation Test:** This assesses stability by comparing the ratio of the standard deviation to the mean across different time periods.

In this study, the ADF test is employed to assess stationarity. The ADF test is an extended form of the unit root test, which refers to a characteristic of a time series where shocks have permanent effects. In the context of the ADF test, if the time series has a unit root, it implies that the series follows a random walk, possibly with drift, does not revert to a long-term mean or trend line, and evaluates whether a unit root exists in a time series.

The general form of the ADF test equation can be written as

$$\Delta y_t = \alpha + \gamma y_{t-1} + \sum_{i=1}^{p-1} \delta_i \Delta y_{t-i} + \epsilon_t \quad (3)$$

where  $\Delta y_t$  denotes the first-order difference in the time series,  $\alpha$  represents the constant term, and  $\gamma$  is the parameter under investigation, corresponding to the coefficient of the lagged value  $y_{t-1}$  of the original time series.  $\delta_i$  is the coefficient of the autoregressive term after differencing, and  $p$  denotes the number of lag periods. The default lag period is given by  $12 \times (\text{nobs}/100)^{(1/4)}$ , where *nobs* refers to the number of observations.  $\epsilon_t$  represents the error term.

The null hypothesis states that the time series contains a unit root and is non-stationary. If the  $p$ -value is below the chosen significance level of 0.05, the  $p$ -value is a measure of the evidence against a null hypothesis. It represents the probability of observing the test statistics or something more extreme, assuming the null hypothesis is true. In the context of the ADF test, a low  $p$ -value suggests strong evidence against the null hypothesis of a unit root. The significance level is a threshold set by the researcher to decide when to reject the null hypothesis. If the null hypothesis is rejected, this indicates that the time series is stationary.

### 3.2. Fitting Results of Wind Speed Distribution

The fitting results of the U-component wind speed probability density distribution in the canyon area are presented in Figure 2 and Table 1, with Table 2 detailing the specific functions of the equations used for fitting. The wind speed in this region exhibits a bimodal distribution, with the main data range spanning 0–8 m/s and peaks occurring at approximately 1 m/s and 5 m/s. Consequently, a mixed distribution model was introduced for fitting. In this mountainous terrain, the mixed distribution model ( $R^2 > 0.99$ ) provides significantly more accurate fitting results compared to the single distribution model ( $R^2 = 0.804$  and  $R^2 = 0.772$ ). Based on the fitting results, the Weibull-Gamma mixed distribution model is recommended for describing wind speed characteristics.

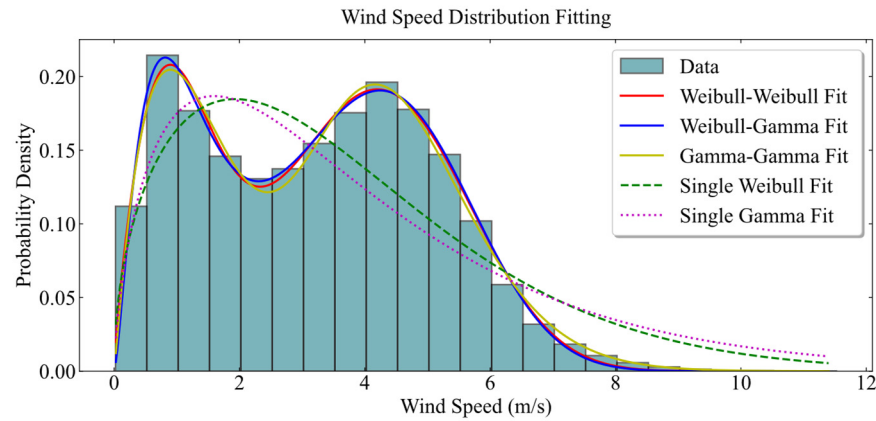


Figure 2. Probability density distribution of wind speed at bridge deck height.

Table 1. Wind speed probability density distribution fitting results.

Distribution	Shape Parameter 1	Scale Parameter 1	Shape Parameter 2	Scale Parameter 2	Weighting Factor of Model 1	R <sup>2</sup>
Weibull	1.498	4.033	\	\	1	0.804
Gamma	1.699	2.28	\	\	1	0.772
Weibull-Weibull	4.666	3.392	1.297	1.817	0.681	0.996
Weibull-Gamma	4.724	3.545	2.494	0.522	0.649	0.998
Gamma-Gamma	2.134	0.792	13.948	0.333	0.465	0.994

\* Take the Weibull-Gamma mixture model as an example. In this model, shape parameter 1 ( $\lambda$ ) and scale parameter 1 ( $k$ ) are the parameters of the first Weibull distribution, while shape parameter 2 ( $\alpha$ ) and scale parameter 2 ( $\beta$ ) are those of the Gamma distribution, and  $\omega$  is the weighting factor of the first Weibull distribution, determining its contribution to the overall mixture.

Table 2. PDFs of wind speed modeling.

Distribution	Probability Density Function (PDF)
Weibull	$f(x; \lambda, k) = \frac{k}{\lambda} \left(\frac{x}{\lambda}\right)^{k-1} \exp\left[-\left(\frac{x}{\lambda}\right)^k\right]$
Gamma	$f(x; \alpha, \beta) = \frac{x^{\alpha-1}}{\beta^\alpha \Gamma(\alpha)} \exp\left(-\frac{x}{\beta}\right)$
Weibull-Weibull	$f(x; \lambda_1, k_1, \lambda_2, k_2, \omega) = \omega \frac{k_1}{\lambda_1} \left(\frac{x}{\lambda_1}\right)^{k_1-1} \exp\left[-\left(\frac{x}{\lambda_1}\right)^{k_1}\right] + (1-\omega) \frac{k_2}{\lambda_2} \left(\frac{x}{\lambda_2}\right)^{k_2-1} \exp\left[-\left(\frac{x}{\lambda_2}\right)^{k_2}\right]$
Weibull-Gamma	$f(x; \lambda, k, \alpha, \beta, \omega) = \omega \frac{k}{\lambda} \left(\frac{x}{\lambda}\right)^{k-1} \exp\left[-\left(\frac{x}{\lambda}\right)^k\right] + (1-\omega) \frac{x^{\alpha-1}}{\beta^\alpha \Gamma(\alpha)} \exp\left(-\frac{x}{\beta}\right)$
Gamma-Gamma	$f(x; \alpha_1, \beta_1, \alpha_2, \beta_2, \omega) = \omega \frac{x^{\alpha_1-1}}{\beta_1^{\alpha_1} \Gamma(\alpha_1)} \exp\left(-\frac{x}{\beta_1}\right) + (1-\omega) \frac{x^{\alpha_2-1}}{\beta_2^{\alpha_2} \Gamma(\alpha_2)} \exp\left(-\frac{x}{\beta_2}\right)$

### 3.3. Characteristics of Fluctuating Wind Under Stationarity Assumption

Turbulence intensity quantifies the relative strength of pulsating wind. It is defined as the ratio of the standard deviation of wind speed fluctuations to the mean maximum wind speed over a 10 min interval:

$$I_u = \frac{\sigma_u}{\bar{U}} \tag{4}$$

In the formula,  $I_\alpha$  denotes the turbulence intensity in three directions, where the subscript  $\alpha$  represents  $u$ ,  $v$  and  $w$ , respectively.  $\sigma_\alpha$  represents the standard deviation of wind speed fluctuations, and  $\bar{U}$  represents the mean wind speed.

Additionally, wind pulsation intensity can also be expressed using the gust factor, typically defined as the ratio of the maximum mean wind speed over a gust duration ( $t_g = 3$ ) to the mean maximum wind speed over a 10 min interval.

$$G_u(t_g) = 1 + \frac{\max[\bar{u}(t_g)]}{\bar{U}} \tag{5}$$

Based on data preprocessing, wind speeds exceeding 4 m/s were selected for pulsating wind calculations. The calculations of turbulence intensity and gust factor are presented in

Figures 3 and 4. Turbulence intensity was primarily distributed in the range of 0.05–0.30 and exhibited an overall decreasing trend with increasing wind speed. Due to significant data dispersion, the linear fitting results were poor.

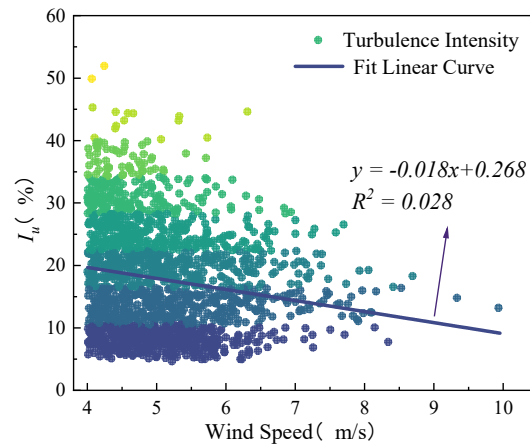


Figure 3. Relationship between turbulence intensity and wind speed.

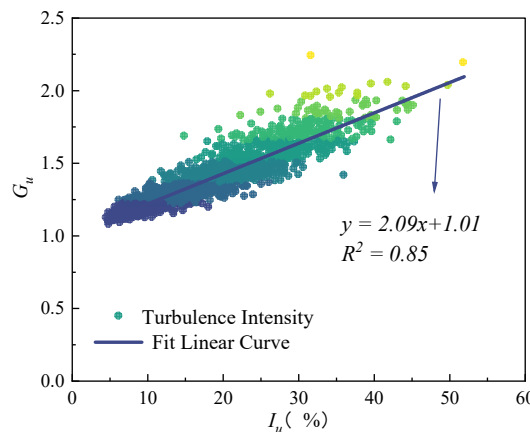


Figure 4. Relationship between gust factor and turbulence intensity.

Gust factors corresponding to turbulence intensity were primarily distributed in the range of 1.0–2.0. The gust factors exhibited an overall upward trend with increasing turbulence intensity, showing strong linear correlation with an  $R^2$  value of 0.85.

### 3.4. Stationarity Tests at Different Heights

To investigate the variation in non-stationary phenomena with height, specifically focusing on the U-component of wind velocity, the stationarity test described in Section 3.1 was conducted at five measurement points along the height, with the results shown in Figure 5. The proportion of non-stationary samples increases from 9.0% at the 20 m measurement point to 31.1% at the 50 m bridge deck height. The overall trend indicates that non-stationarity gradually increases with height.

More non-stationary samples are observed at the 10 m measurement point, likely due to strong non-stationarity near the surface, influenced by objects such as vegetation and stones. The high proportion of non-stationary sample sequences in the canyon area can be attributed to the following reasons: First, terrain features such as ridges and canyons induce rapid changes in wind speed and direction, leading to the generation of non-stationary winds. Secondly, the mountainous wind field contains both large-scale eddy circulations and small-scale turbulence, with this multi-scale characteristic exhibiting non-stationarity in wind speed analysis. In general, sudden changes in wind speed and gusts caused by mountainous terrain may result in the non-stationary characteristics of wind speed.

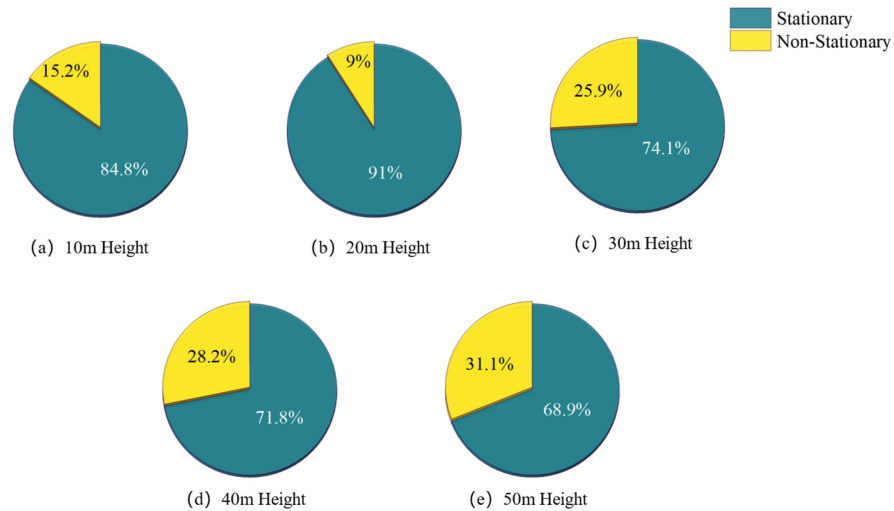


**Figure 5.** Results of stationarity tests at different heights.

### 3.5. Fluctuating Wind Characteristics of Different Wind Speed Model

Based on the above research findings, the wind speed at the bridge deck height in this area exhibits significant non-stationarity. Therefore, the pulsating wind characteristics of different wind speed samples were compared and analyzed.

Figure 6 compares the variations in turbulence intensity with wind speed between the two samples. The turbulence intensity of both samples shows a negative correlation, decreasing with increasing wind speed, and exhibits substantial dispersion. The distribution patterns of the two sample types are largely consistent, and the linear fitting results are similar, with minimal differences in slope and intercept.

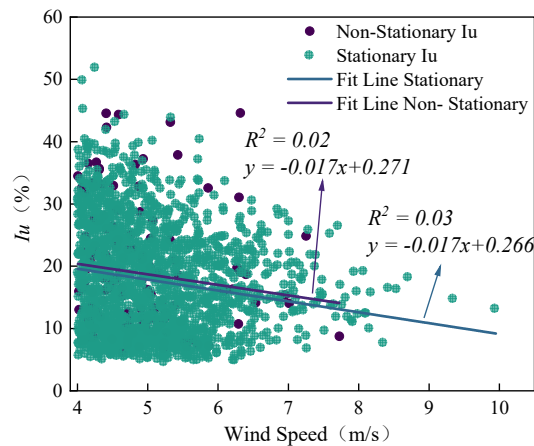


**Figure 6.** Relationship between wind speed and turbulence for different models.

A comparison of the variation in gust factors with turbulence intensity between the two sample types is shown in Figure 7. Both show a similar positive correlation; however, the slope of the fitting results for stationary samples is slightly greater than that of non-stationary samples. This indicates that the pulsating wind characteristics of different wind speed samples vary to some extent.

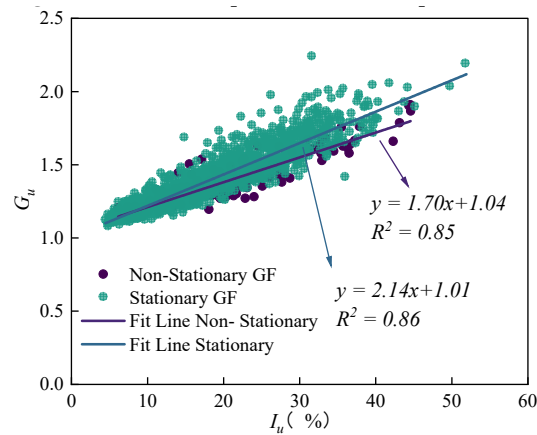


Figure 7. Relationship between gust factor and turbulence for different models.

### 4. DWT Reconstruction and Analysis

#### 4.1. DWT Analysis Process and Theory

Based on the above studies, it is evident that the non-stationary model influences the pulsating wind characteristics in the canyon area. To further evaluate its impact, the wavelet transform (WT) method, commonly applied in analyzing non-stationary signals, is introduced. Discrete wavelet transform (DWT), a specific form of wavelet transform, decomposes a signal into wavelet coefficients at different scales, capturing its local characteristics.

The widely used db10 wavelet DWT was adopted in this study [12,22,23] to extract time-varying mean wind speed and analyze the effects of different decomposition levels. The decomposition process is illustrated in Figure 8.

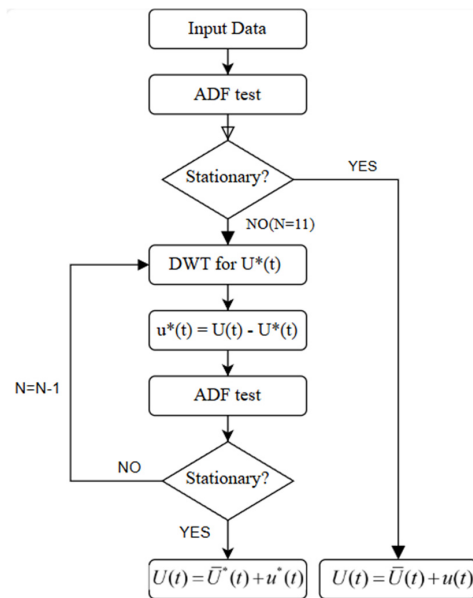


Figure 8. Flowchart illustrating the wavelet decomposition and reconstruction steps.

The DWT db10 decomposition method decomposes the signal using a set of low-pass filters  $h[n]$  and high-pass filters  $g[n]$ . The db10 wavelet has predefined values for the coefficients of both the low-pass and high-pass filters. Given a signal sequence  $x[n]$ , the db10 wavelet decomposition can be mathematically expressed as follows:

$$A_j[m] = \sum_n x[n] \cdot h[2m - n] \tag{6}$$

$$D_j[m] = \sum_n x[n] \cdot g[2m - n] \tag{7}$$

$A_j[m]$  is the approximation coefficients and  $D_j[m]$  is the detail coefficients;  $j$  represents the decomposition depth (level). To reconstruct and calculate the time-varying mean wind at different levels, it is necessary to convolve the low-frequency coefficients  $A_j[m]$  and high-frequency coefficients  $D_j[m]$  of that level with the corresponding filter coefficients. The reconstruction can be expressed as

$$A_{j-1}[n] = \sum_m (A_j[m] \cdot h_r[2m - n] + D_j[m] \cdot g_r[2m - n]). \tag{8}$$

The symbol  $A_{j-1}[n]$  denotes the reconstruction outcome at the current decomposition level, accounting for boundary effects. In this study, the maximal decomposition depth  $N_0$  is established at 11, a parameter determined through Equation 9. This equation is derived from the principles of decomposition as described by the Mallat algorithm [24].

$$N_0 = \log_2(T \cdot s) \tag{9}$$

$N_0$  denotes the maximum decomposition level of the discrete wavelet transform (DWT);  $T$  represents the time interval; and  $s$  indicates the sampling frequency of the wind record.

For the imported samples, those passing the ADF stationarity test at a significance level of 0.05 were directly averaged and analyzed based on the original stationarity hypothesis. For samples failing the test, the db10 wavelet basis was used to decompose the original wind speed data  $U(t)$ , reconstruct the low-frequency component  $U^*(t)$ , and adjust the time-varying mean wind speed. The reconstructed component  $U^*(t)$  is subtracted from  $U(t)$  to obtain the pulsating wind speed  $u^*(t)$ , which is then subjected to a stationarity test. If stationarity is not achieved, the process iterates with  $N-1$ .

To comprehensively analyze the time series characteristics of pulsating wind under different orders and verify the effectiveness of wavelet decomposition, this study employed the ACF and PACF methods to identify autocorrelation and partial autocorrelation in the pulsating wind sequence. This ensures that the extracted pulsating wind accurately represents the medium- and high-frequency fluctuations in the original signal, thereby providing a foundation for further predictions and analyses.

The autocorrelation function (ACF) test is a method for analyzing time series data. It measures the correlation of a signal with itself over specified time delays. For time series data, the ACF reveals linear dependencies between data points, particularly the degree of correlation between adjacent points. For a time series  $\{X_t\}$ , the autocorrelation coefficient  $r_k$  is defined at lag  $k$  is defined as

$$r_k = \frac{\sum_{t=k+1}^n (X_t - \mu)(X_{t-k} - \mu)}{\sum_{t=1}^n (X_t - \mu)^2} \tag{10}$$

where  $\mu$  is the mean of the time series and  $n$  is the length of the time series. The autocorrelation coefficient ranges from  $-1$  to  $1$ . A value closer to  $1$  indicates a stronger positive correlation, while a value closer to  $-1$  indicates a stronger negative correlation. A value near  $0$  suggests a weak correlation. The autocorrelation function (ACF) plot illustrates the variation in the autocorrelation coefficient as the lag ( $k$ ) increases. By examining the ACF plot, one can assess whether the time series exhibits a periodic pattern or trend. For time series with periodicity, the ACF typically displays prominent peaks at multiples of the period.

The partial autocorrelation function (PACF) test is a statistical tool for time series analysis, which measures the degree of direct correlation between two time points after excluding the influence of the intermediate lag term. PACF helps to identify and quantify net correlations between different time points in a time series. For the time series  $\{X_t\}$ , the partial autocorrelation coefficient at lag  $k$ , denoted as  $\varphi_{kk}$ , can be understood as the strength of the linear relationship between  $X_t$  and  $X_{t-k}$ , while controlling for the intermediate lags  $X_{t-1}, X_{t-2}, \dots, X_{t-(k-1)}$ .

$$X_t = \varphi_1 X_{t-1} + \varphi_2 X_{t-2} + \dots + \varphi_p X_{t-k} + \epsilon_t \tag{11}$$

$\epsilon_t$  is white noise.  $\varphi_{kk}$  is calculated by solving the following Yule-Walker equations.

$$\begin{pmatrix} r_1 \\ r_2 \\ \vdots \\ r_k \end{pmatrix} = \begin{pmatrix} 1 & r_1 & \dots & r_{k-1} \\ r_1 & 1 & \dots & r_{k-2} \\ \vdots & \vdots & \ddots & \vdots \\ r_{k-1} & r_{k-2} & \dots & 1 \end{pmatrix} \begin{pmatrix} \varphi_1 \\ \varphi_2 \\ \vdots \\ \varphi_k \end{pmatrix} \tag{12}$$

In this context,  $r_i$  denotes the autocorrelation coefficient at lag  $i$ . The partial autocorrelation function (PACF) plot is useful for assessing the strength of long-term relationships while controlling for short-term fluctuations. If the PACF approaches 0 at multiple lags, the direct linear correlation between time points in the time series is weak. In contrast to the ACF, the PACF emphasizes direct correlations over indirect ones. Moreover, in the analysis of pulsating wind characteristics, the gust duration ( $t_g$ ) is typically 3 s; thus, the 3-s time series results are primarily considered in ACF and PACF analysis.

#### 4.2. DWT Reconstruction Results

In the analysis of 1669 ten-minute wind speed samples with U-component speeds exceeding 4 m/s at bridge deck height, all fluctuating wind speed samples reconstructed using db10 wavelet decomposition at levels greater than or equal to 9 passed the ADF stationarity test at a significance level of 0.05. Figure 9 illustrates the reconstruction results of selected samples at various decomposition levels.

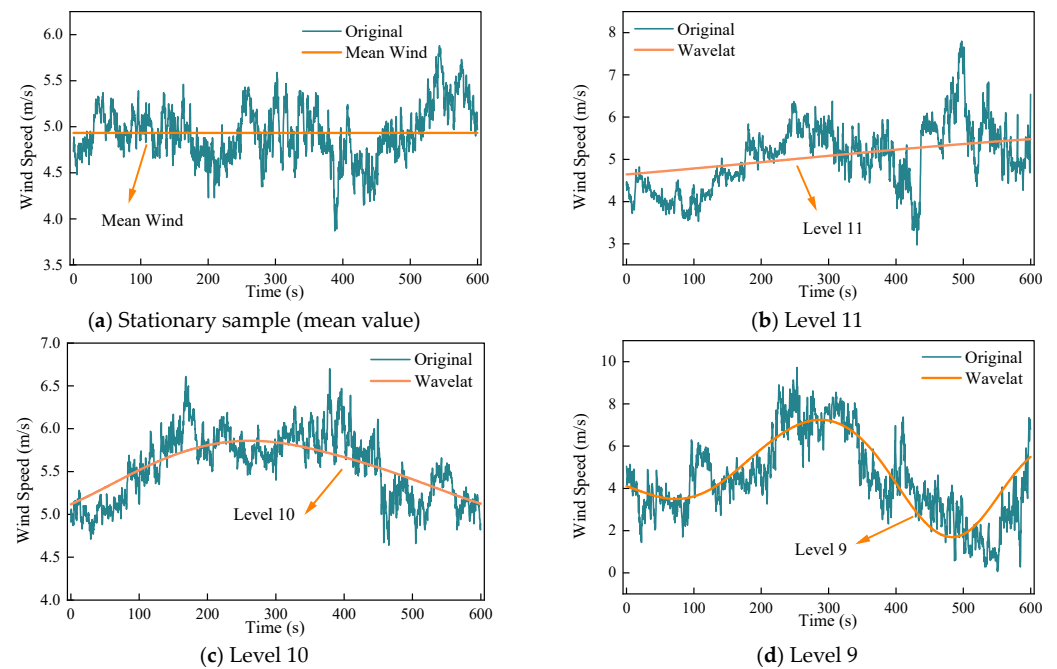
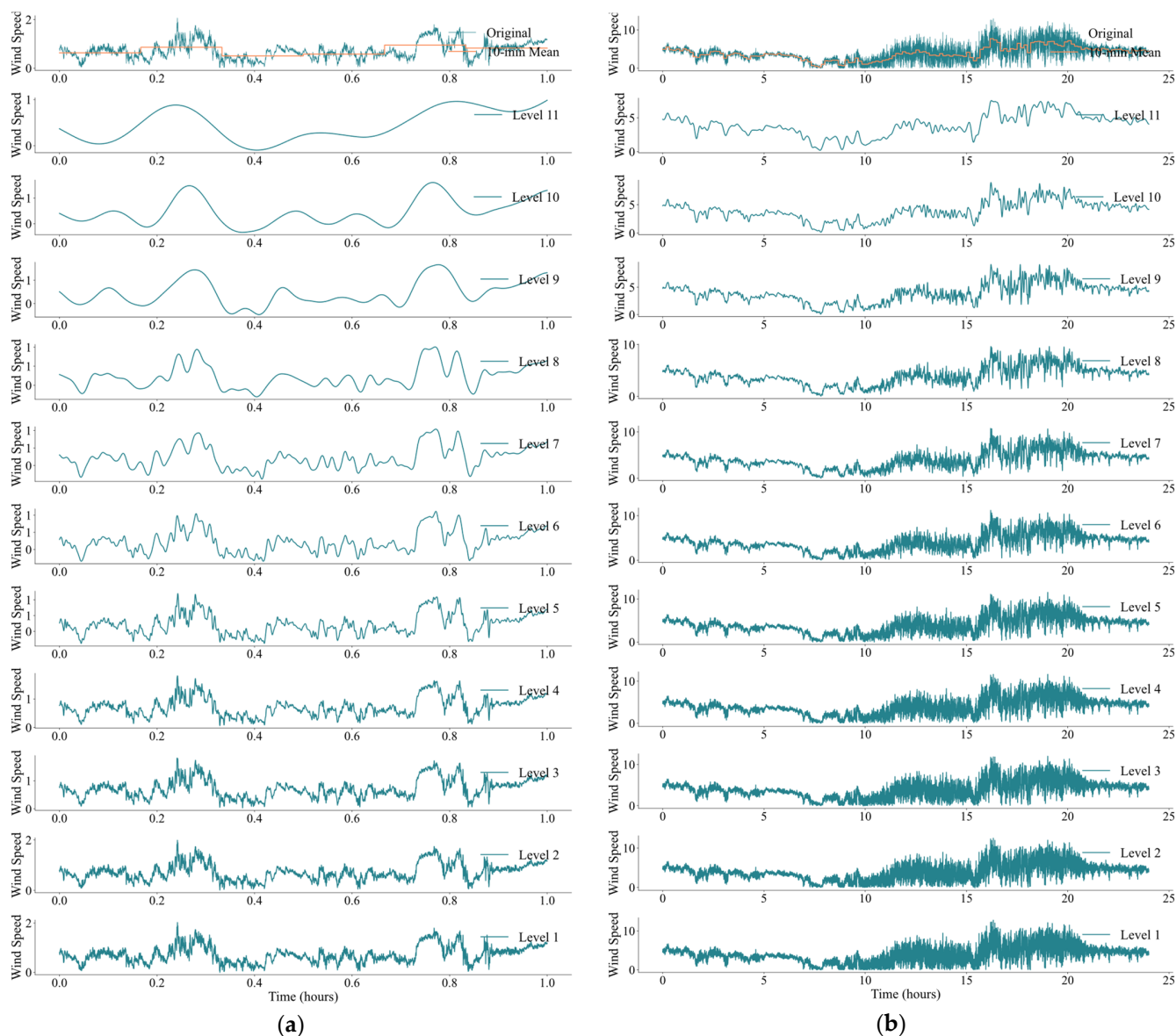


Figure 9. Comparison of wavelet reconstruction results across different decomposition levels.

To further examine the impact of different decomposition levels on pulsating wind speed characteristics, the wavelet components at levels 1 through 11 were reconstructed, as shown in Figure 10. As the decomposition level decreases, the overall fluctuation trend becomes increasingly apparent, and the instantaneous wind speed variability becomes clearer. This indicates that when using the wavelet method, selecting an appropriate number of wavelet levels is crucial.



**Figure 10.** DWT reconstruction results for the sample: (a) hour, (b) day.

If the decomposition level is too low, excessively detailed time-varying mean wind components may be extracted, leading to the loss of fluctuating wind characteristics.

#### 4.3. Optimal Decomposition Level for DWT

To investigate the changes in the autocorrelation and partial autocorrelation of pulsating wind after wavelet decomposition at each level, the ACF and PACF test methods introduced in Section 4.1 were employed for calculation and analysis. Figure 11 illustrates the correlation between the wavelet-decomposed signal at each level and its adjacent data points.

The pulsating wind characteristics under different wavelet decomposition levels exhibit notable differences: Level 3 showed rapid attenuation and periodic oscillations in ACF, approaching 0 after 4 s, while levels 5, 7, and 9 displayed a more gradual attenuation trend and stabilized at a certain value. The PACF results indicate that all levels decay rapidly to nearly 0 within a very short lag, suggesting that the correlation of adjacent data persists for only about two sample intervals, or approximately 0.5 s. Comparison of ACF and PACF results suggests that the wind retains a large-scale pulsating structure at levels 5–9, which is presumed to correspond to a coherent structure of turbulence. However, level 3 disrupts the coherent structure in the turbulent flow, making it unsuitable for analyzing pulsating wind characteristics.

Figure 12 presents the power spectral density analysis results for each wavelet decomposition level. Power spectral density analysis reveals that reconstruction results for level 5 and above converge near 0.05 Hz, with these wavelets significantly influencing wind above this frequency. In contrast, reconstruction at level 3 primarily affects the medium- and high-frequency components of pulsating wind. Thus, improper level selection significantly alters the characteristics of reconstructed pulsating wind.

Comparison with the original data power spectral density reveals that levels 5–9 consistently preserve high-frequency wind components, effectively remove low-frequency large-scale wind, and retain the middle- and high-frequency structures. Therefore, selecting levels 5–9 in the measured data is considered reasonable.

Additionally, comparative analysis of Figures 13 and 14 indicates that levels 7 and 9 exhibit a gradual rising trend in the power spectral density and retain some low-frequency components, whereas the level 5 wavelet eliminates low-frequency wind more effectively and better preserves the coherent structures of turbulence. Thus, the level 5 wavelet is recommended for decomposing and reconstructing the time-varying mean wind in this study.

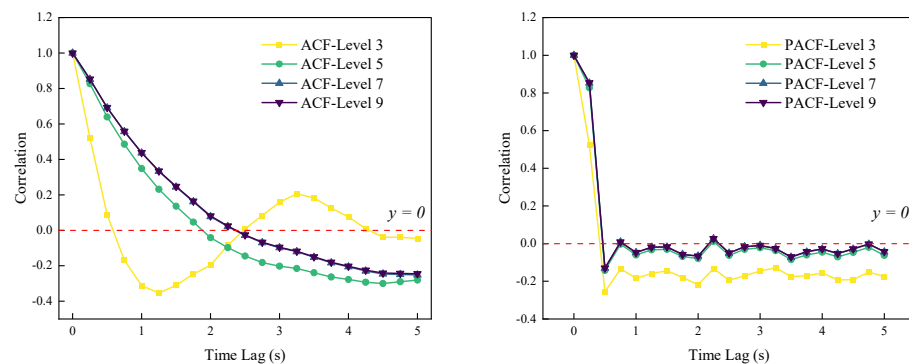


Figure 11. Analysis of ACF and PACF.

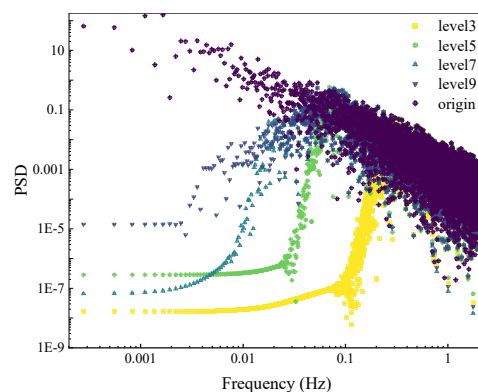


Figure 12. PSD at different levels across different decomposition levels.

#### 4.4. Analysis of Non-Stationary Wind Data Using Optimal Decomposition Levels in DWT

To compare and analyze the differences in turbulence intensity, turbulence integral scale, and turbulent power spectral density between pulsating wind extracted from the time-varying mean wind after wavelet decomposition and pulsating wind calculated under the stationary assumption, wind speed samples from the middle bridge deck height on August 6 were selected. These samples passed the ADF stationarity test at a significance level of 0.05 when the decomposition process reached level 9.

The “db10” wavelet at the optimal decomposition level (level 5) identified in the previous study was selected to reconstruct the sample data. Figure 13 illustrates the reconstruction results for selected periods of the U-component wind speed sample.

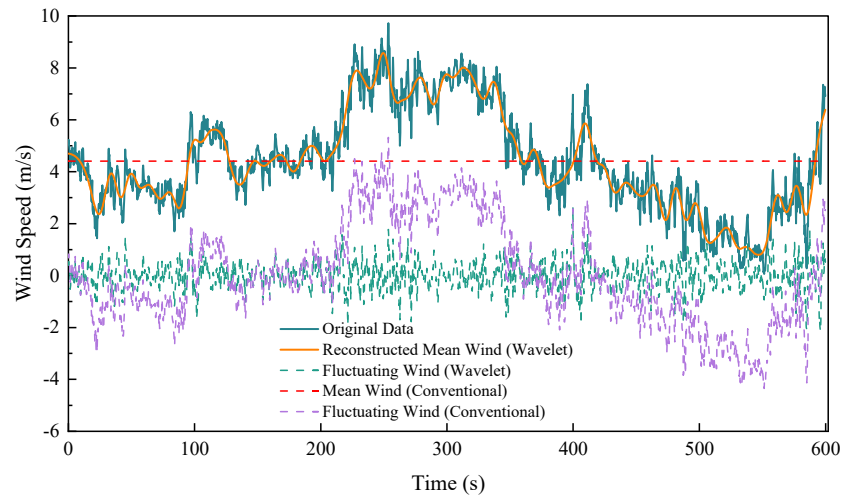


Figure 13. DWT reconstruction results for the sample at level 5.

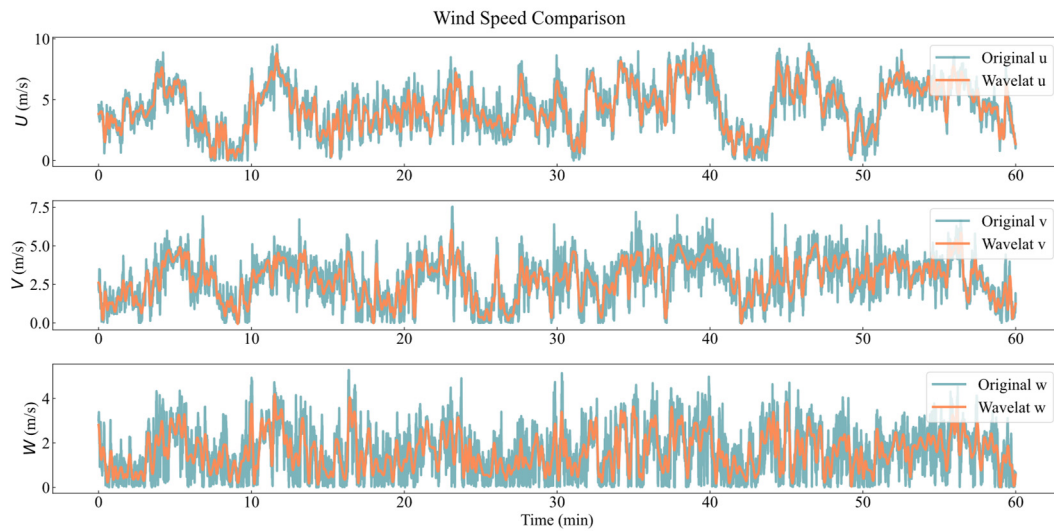


Figure 14. Time-varying mean wind from wavelet reconstruction and original wind speed.

Although the definition and calculation method of the non-stationary wind speed model are consistent, the parameters correspond specifically to the non-stationary wind speed model. The calculation formula is given as

$$I_{\alpha}^* = \frac{\sigma_{\alpha}^*}{U_*} (\alpha = u, v, w) \tag{13}$$

where  $I^*_\alpha$  is the turbulence intensity in three directions, and the subscript  $\alpha$  represents  $u, v,$  and  $w,$  respectively.  $\sigma^*_\alpha$  denotes the standard deviation of wind speed fluctuations and  $U^*$  represents the time-varying mean wind speed.

The turbulence integral scales of the stationary and non-stationary models are calculated as follows:

$$L_\alpha = \frac{U}{\sigma_\alpha^2} \int_0^\infty R_\alpha(\tau) d\tau, (\alpha = u, v, w) \tag{14}$$

$$L^*_\alpha = \frac{\bar{U}^*}{\sigma_\alpha^{*2}} \int_0^\infty R^*_\alpha(\tau) d\tau, (\alpha = u, v, w) \tag{15}$$

$L_\alpha$  and  $L^*_\alpha$  denote the integral scales of stationary and non-stationary turbulence, respectively, while  $R_\alpha$  and  $R^*_\alpha$  represent the autocovariance functions of stationary and non-stationary fluctuations, respectively. To account for large errors caused by Taylor’s hypothesis when autocovariance is small, it is recommended to limit the integral to the first  $t,$  where  $R_\alpha(\tau) = 0.05\sigma_\alpha^2$  or  $R_\alpha(\tau) = 0.05(\sigma^*_\alpha)$  [25].

Based on the two different wind speed models, the turbulence intensity and integral scale in the  $u, v,$  and  $w$  directions at the 50 m bridge deck height within a 1 h sample are illustrated in Figure 15. The results indicate that turbulence intensity under the stationary wind speed model is higher than that under the non-stationary wind speed model, suggesting that the stationary wind speed model overestimates turbulence in non-stationary wind, consistent with findings by Ren et al. [12].

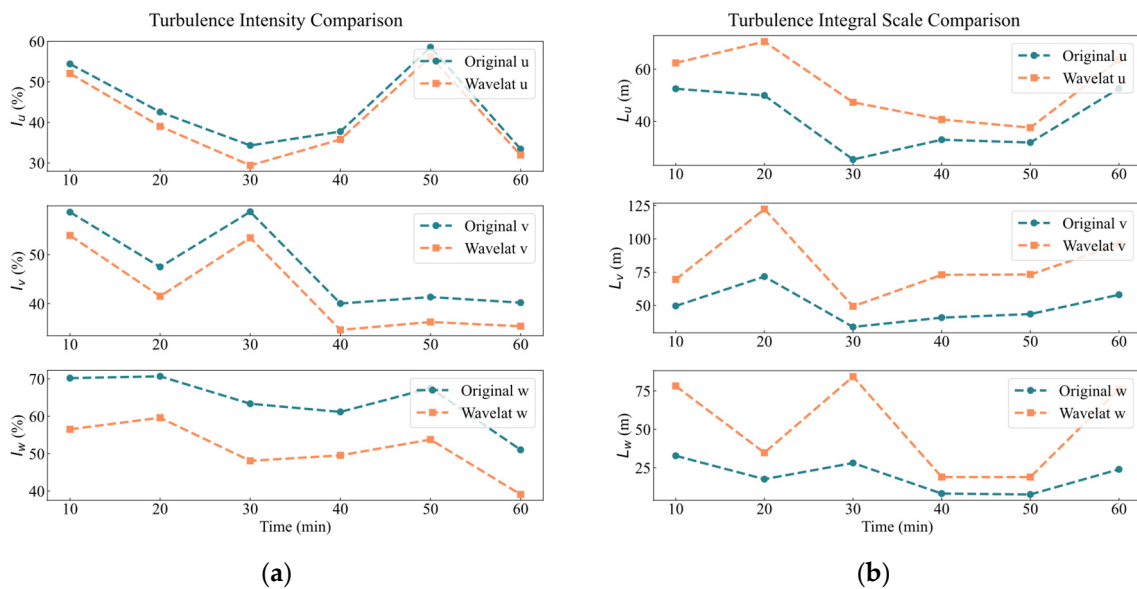


**Figure 15.** Analysis of different wind speed models: (a) turbulence intensity (b) turbulence integral scale.

However, the turbulence integral scale exhibits slight differences: the stationary wind speed model yields a lower turbulence integral scale compared to the non-stationary model. When trends or periodic changes in actual wind speed are present, the stationary model interprets these changes as random fluctuations, thereby increasing the standard deviation of velocity fluctuations and resulting in higher turbulence.

An inverse relationship exists between the turbulence integral scale and turbulence intensity. This indicates that analyses based on the stationary assumption may misinterpret some large-scale structures as fluctuating components, thereby increasing the standard deviation and failing to accurately capture long-term correlations or large-scale structures.

Figure 16 illustrates the reconstructed power spectral density of the sample under different wind speed models. The reconstructed power spectral density results demonstrate that wavelet reconstruction effectively removes low-frequency structures from the wind.

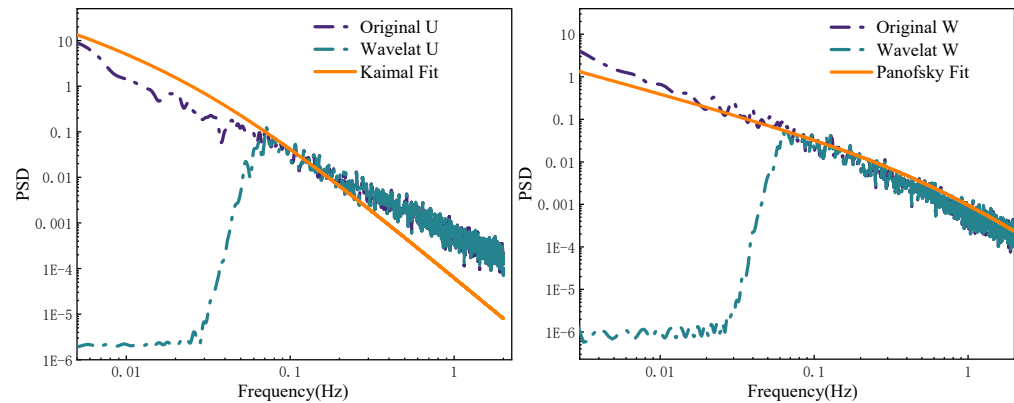


Figure 16. PSD analysis comparing original and reconstructed fluctuating wind.

The distribution of turbulent energy is defined by the turbulent wind spectrum in the frequency domain. According to the Chinese wind resistance specification, the Kaimal spectrum is applied to the longitudinal power spectrum, while the Panofsky spectrum is used for the vertical power spectrum. The Kaimal and Panofsky power spectra are described by formulas (9) and (10), respectively.

$$\frac{nS_u(n)}{(u_*)^2} = \frac{200f}{(1 + 50f)^{5/3}} \tag{16}$$

$$\frac{nS_w(n)}{u_*^2} = \frac{6f}{(1 + 4f)^2} \tag{17}$$

$n$  is the frequency of wind (Hz),  $u_*$  is the friction velocity, and  $f$  is the Monin similarity coordinate.  $S_u(n)$  is the wind power spectrum.

The longitudinal wind spectrum and the Kaimal spectrum exhibit inconsistencies at both low and high frequencies. At low frequencies, the measured wind spectrum under the stationary wind speed model is lower than the Kaimal spectrum. At high frequencies, the measured and reconstructed wind spectra are significantly higher than the Kaimal spectrum, suggesting that the energy contribution of small vortex structures in the measured wind field is not well captured by the Kaimal spectrum.

The vertical wind spectrum exhibits relatively strong consistency with the Panofsky spectrum. At low frequencies, the vertical wind spectra measured under the stationary wind speed model are slightly higher than the Panofsky spectrum, whereas at high frequencies, they align well with the Panofsky spectrum.

### 5. Conclusions

This study examines the pulsating wind characteristics at the U-shaped canyon bridge site in Yunnan Province, introduces non-stationary theory and associated analysis methods, and analyzes the pulsating wind from various perspectives. These include the differences in pulsating wind characteristics caused by different models, the stationarity test at various heights, and research on the optimal decomposition level for DWT. The conclusions are as follows:

- (1) Wind speed in the canyon area exhibits bimodal distribution characteristics, and the Weibull-Gamma mixed distribution model achieves the best fit, with  $R^2 = 0.998$ .

- (2) Under the stationary hypothesis, the turbulence intensity is mainly distributed in the range of 0.05–0.30 and decreases with the increase in wind speed. The gust factor is mainly distributed in the range of 1.0–2.0, and has a strong linear correlation with turbulence intensity ( $R^2 = 0.85$ ).
- (3) Stationarity analysis reveals that the proportion of non-stationary sequences in mountainous areas increases with height. Wavelet decomposition shows that all pulsating wind samples reconstructed at levels greater than nine pass the stationarity test. Further analysis indicates that the extraction of time-varying mean wind is most effective at level 5 decomposition.
- (4) The reconstruction results of non-stationary samples indicate that the stationary wind speed model overestimates turbulence intensity under non-stationary conditions but underestimates the turbulence integral scale. This suggests that the stationary model may fail to accurately capture long-term correlations or large-scale structures due to its assumption of stationarity. Therefore, non-stationary analysis is essential for mountainous regions.
- (5) Power spectral density analysis demonstrates that wavelet reconstruction effectively removes the low-frequency components of the wind. However, a comparison with classical theoretical spectra reveals a certain degree of deviation between the measured wind spectrum and the theoretical models.

This study, based on measured data from the U-shaped canyon bridge site, aims to identify and reveal the primary characteristics of the pulsating wind in the canyon, expand the wind field data for the area, and provide valuable references for the structural wind resistance design in canyon regions. In bridge design, studying non-stationary wind characteristics helps engineers optimize wind resistance strategies for mountain bridges, enhancing their wind resistance and reducing the risk of wind-induced disasters. Additionally, the research results can inform wind-related projects such as wind power generation in mountainous areas. In the future, more measurement points could be added to the bridge site to explore more comprehensive wind characteristics and extend the research to other complex terrains to verify and expand the current findings.

**Author Contributions:** Conceptualization, Z.S. and F.W.; methodology, Z.S. and F.W.; software, Z.S.; validation, J.W., Z.Z. and X.Z.; formal analysis, Z.S.; investigation, Z.S., J.W. and Z.Z.; resources, F.W.; data curation, F.W.; writing—original draft preparation, Z.S. and Z.Z.; writing—review and editing, J.W., X.Z. and Z.Z.; visualization, Z.S. and X.Z.; supervision, J.W.; project administration, F.W.; funding acquisition, F.W. All authors have read and agreed to the published version of the manuscript.

**Funding:** This research received no external funding.

**Institutional Review Board Statement:** Not applicable.

**Informed Consent Statement:** Not applicable.

**Data Availability Statement:** The original contributions presented in the study are included in the article; further inquiries can be directed to the corresponding author.

**Conflicts of Interest:** The authors declare no conflicts of interest.

## Abbreviations

The following abbreviations are used in this manuscript:

DWT	Discrete wavelet transform
ADF	Augmented Dickey–Fuller
ACF	Autocorrelation function
PACF	Partial autocorrelation function
PSD	Power spectral density

## References

- Liao, H.; Jing, H.; Ma, C.; Tao, Q.; Li, Z. Field measurement study on turbulence field by wind tower and Windcube Lidar in mountain valley. *J. Wind. Eng. Ind. Aerodyn.* **2020**, *197*, 104090. [CrossRef]
- Shen, Z.; Li, J.; Li, R.; Gao, G. Nonuniform wind characteristics and buffeting response of a composite cable-stayed bridge in a trumpet-shaped mountain pass. *J. Wind. Eng. Ind. Aerodyn.* **2021**, *217*, 104730. [CrossRef]
- Hui, Y.; Tang, Y.; Yang, Q.; Chen, B. A wake-oscillator model for predicting VIV of 4-to-1 rectangular section cylinder. *Nonlinear Dyn.* **2024**, *112*, 8985–8999. [CrossRef]
- Li, J.; Yang, S.; Hao, J.; Gao, G.; Wang, F.; Bai, H.; Zhao, G.; Li, Y.; Xue, X. Advances and applications of wind engineering in exceptional terrain. *J. Traffic Transp. Eng.* **2024**, *11*, 1023–1209. [CrossRef]
- Wu, F.; Cui, W.; Zhao, L.; Guo, Z.; Li, Q.; Ge, Y. Field Measurements of Wind Microclimate at the Vehicle Level on a Bridge Deck under Typical Canyon Terrain. *J. Bridge Eng.* **2023**, *28*, 04023013. [CrossRef]
- Hao, J.; Zhao, S.; Xin, L.; Zhao, X.; Wang, F.; Li, J. Study on wind characteristics of bridge sites in coastal areas of Guang-dong Province based on measured data. *J. Vib. Eng.* **2024**, 1–9. Available online: <https://link.cnki.net/urlid/32.1349.tb.20240202.0944.002> (accessed on 15 January 2025). (In Chinese).
- Li, Y.; Hu, P.; Xu, X.; Qiu, J. Wind characteristics at bridge site in a deep-cutting gorge by wind tunnel test. *J. Wind. Eng. Ind. Aerodyn.* **2017**, *160*, 30–46. [CrossRef]
- Song, J.-L.; Li, J.-W.; Flay, R.G.J.; Pirooz, A.A.S.; Fu, J.-Y. Validation and application of pressure-driven RANS approach for wind parameter predictions in mountainous terrain. *J. Wind. Eng. Ind. Aerodyn.* **2023**, *240*, 105483. [CrossRef]
- Song, J.-L.; Li, J.-W.; Flay, R.G.J. Field measurements and wind tunnel investigation of wind characteristics at a bridge site in a Y-shaped valley. *J. Wind. Eng. Ind. Aerodyn.* **2020**, *202*, 104199. [CrossRef]
- He, Y.C.; Chan, P.W.; Li, Q.S. Wind characteristics over different terrains. *J. Wind. Eng. Ind. Aerodyn.* **2013**, *120*, 51–69. [CrossRef]
- Zhang, J.; Zhang, M.; Li, Y.; Jiang, F.; Wu, L.; Guo, D. Comparison of wind characteristics in different directions of deep-cut gorges based on field measurements. *J. Wind. Eng. Ind. Aerodyn.* **2021**, *212*, 104595. [CrossRef]
- Ren, W.; Pei, C.; Ma, C.; Li, Z.; Wang, Q.; Chen, F. Field measurement study of wind characteristics at different measuring positions along a bridge in a mountain valley. *J. Wind. Eng. Ind. Aerodyn.* **2021**, *216*, 104705. [CrossRef]
- Jing, H.; Liao, H.; Ma, C.; Tao, Q.; Jiang, J. Field measurement study of wind characteristics at different measuring positions in a mountainous valley. *Exp. Therm. Fluid Sci.* **2020**, *112*, 109991. [CrossRef]
- Huang, G.; Jiang, Y.; Peng, L.; Solari, G.; Liao, H.; Li, M. Characteristics of intense winds in mountain area based on field measurement: Focusing on thunderstorm winds. *J. Wind. Eng. Ind. Aerodyn.* **2019**, *190*, 166–182. [CrossRef]
- Li, Y.; Jiang, F.; Zhang, M.; Dai, Y.; Qin, J.; Zhang, J. Observations of periodic thermally-developed winds beside a bridge region in mountain terrain based on field measurement. *J. Wind. Eng. Ind. Aerodyn.* **2022**, *225*, 104996. [CrossRef]
- Guo, Z.; Hu, Z.; Ma, T.; Huang, X. Wavelet characterizing the non-stationary features of mountain valley winds both in frequency and time domain. *J. Wind. Eng. Ind. Aerodyn.* **2023**, *243*, 105611. [CrossRef]
- Niu, H.; Cao, N.; Li, H.; Jiang, D.; Chen, Z. Measurement and Non-Stationary Characteristics Analysis of Near-Ground Wind Fields Below 10 m Height in Hilly Regions. *J. Southeast Univ. (Nat. Sci. Ed.)* **2024**, *54*, 836–844. (In Chinese)
- Xin, Y.; Liu, Z.; Shao, X.; Lu, S. Non-stationary and non-Gaussian features of mountain terrain measured wind. *J. Vib. Shock* **2018**, *37*, 247–252. (In Chinese)
- Zhou, W.; Lou, W.; Huang, M.; Liu, J.; Liang, M. Two-year wind field measurements near the ground at a site of the Tibetan Plateau. *J. Wind. Eng. Ind. Aerodyn.* **2024**, *245*, 105636. [CrossRef]
- Lou, W.; Zhou, W.; Liu, J.; Liang, M.; Cai, K.; Huang, M. Wind Field Measurements in the Tibetan Plateau and Study of Non-Stationary Wind Characteristics. *J. Southeast Univ. (Nat. Sci. Ed.)* **2023**, *53*, 575–584. (In Chinese)
- Ligeza, P.; Jamróz, P.; Socha, K. Development Trends of Air Flow Velocity Measurement Methods and Devices in Renewable Energy. *Energies* **2025**, *18*, 412. [CrossRef]
- Jiang, F.; Zhang, M.; Li, Y.; Yan, T.; Zhang, J. Field measurement analysis of wind parameters and nonstationary characteristics in mountainous terrain: Focusing on cooling windstorms. *J. Wind. Eng. Ind. Aerodyn.* **2022**, *230*, 105175. [CrossRef]

23. Tao, T.; Wang, H.; Wu, T. Comparative Study of the Wind Characteristics of a Strong Wind Event Based on Stationary and Nonstationary Models. *J. Struct. Eng.* **2017**, *143*, 04016230. [[CrossRef](#)]
24. Mallat, S. Multiresolution approximations and wavelet orthonormal bases of  $L_2(\mathbb{R})$ . *Trans. Am. Math. Soc.* **1989**, *315*, 69–88.
25. Flay, R.G.J.; Stevenson, D.C. Integral length scales in strong winds below 20 m. *J. Wind. Eng. Ind. Aerodyn.* **1988**, *28*, 21–30. [[CrossRef](#)]

**Disclaimer/Publisher’s Note:** The statements, opinions and data contained in all publications are solely those of the individual author(s) and contributor(s) and not of MDPI and/or the editor(s). MDPI and/or the editor(s) disclaim responsibility for any injury to people or property resulting from any ideas, methods, instructions or products referred to in the content.